A Virtual Excavator for Controller Development and Evaluation

S. P. DiMaio, S. E. Salcudean, C. Reboulet†, S. Tafazoli and K. Hashtrudi-Zaad
Department of Electrical and Computer Engineering, University of British Columbia
Vancouver, BC, V6T 1Z4, Canada
{*tims@ece.ubc.ca, simond@ece.ubc.ca*}

† ONERA-CERT, 2 avenue Edouard Belin, 31055 Toulouse, France

Abstract

In order to facilitate the testing and evaluation of control strategies and operator environments designed for heavy duty hydraulic machines, an excavator simulator has been developed and is described in this paper. The simulator comprises an impedance model of the excavator arm, a model for the bucket-ground interaction forces, a graphical environment and a haptic interface. This paper describes the simulator components and their integration.

1 Introduction

Many thousands of excavator-based machines are produced worldwide each year for use in the construction, forestry and mining industries. Improvements in the control algorithms and user interfaces of such machines could lead to substantial productivity gains [18]. In particular, since a significant portion of the work performed by such machines involves interaction with the environment, the use of impedance/force control and force-feedback teleoperation have been proposed and demonstrated [9, 8, 11]. In order to avoid the expensive operation of such machines until it is absolutely necessary, a simulator suitable for experimentation with user interfaces, control strategies and operator training, has been developed at the University of British Columbia (UBC). This simulator comprises machine dynamics as an impedance model, a ground-bucket interaction model, and a graphical display subsystem, all of which are described in this paper. A haptic interface and a cab-motion simulator are also part of the system and have been described elsewhere [14, 13, 16]. The system is shown schematically in Figure 1.

Although virtual environments have been presented previously, particularly for the purpose of master-side interaction within delayed, or low-bandwidth teleoperation applications [3], the authors are not aware of any similar implementations within the excavation field. Simpler simulators for human factors studies, employing essentially no environment dynamics, have been developed for other excavator-based machines, such as log-loaders [18] and feller bunchers [8]. The primary advantage of such systems has been in providing the operator with visual feedback, and in some cases kinesthetic feedback, during periods in which such sensory information cannot be derived from the remote environment [2]. One difficulty experienced in their design has been in the development of accurate and computationally tractable environment models. For digging, the present consensus is that one can expect to obtain only order-of-magnitude force predictions. Indeed, the soil may be non-homogeneous and its mechanical properties poorly defined [15]. Previous interaction force models have included *cutting resistance*, *soil-tool friction*, *soil-soil friction*, *soil mass inertia* and *shearing force* components [1, 4, 7]. Many of these models are described by empirically determined parameters for particular bucket geometries and optimal angles-of-attack. Therefore these are not generally suitable for the purpose of simulation, since they do not provide adequate insight into interaction forces experienced over arbitrary bucket trajectories. In this paper, we present a simple and intuitive ground interaction model which is based upon *stiffness*, *damping*, *inertial* and *shearing* forces. Its goal is to provide qualitatively accurate force feedback during real time virtual environment interaction. This model should be seen as a starting point which, due to the variability of soil parameters, is likely to benefit from estimation techniques, such as extended Kalman filters, for online force estimation within physical environments.

The paper is organised as follows: Section 2 describes the overall system architecture, Section 3 presents the mini-excavator used in the authors' experiments, as well as its impedance model based on

experimental data; thereafter Section 4 describes the ground interaction model, while Section 5 addresses issues of graphical simulation and visual feedback. Section 6 presents conclusions and plans for future work.

2 Simulator Architecture

The simulator system comprises three significant hardware components, namely a Silicon Graphics Iris workstation, a real-time VME system including a SPARCengine processor running the VxWorks^{TM} operating system and a 6-DOF magnetically levitated force feedback joystick [14], as arranged in Figure 1. The excavator and environment dynamics, as well as

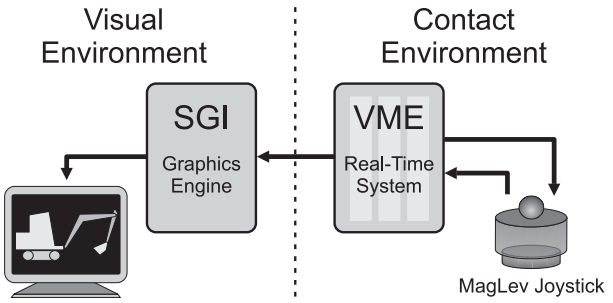

Figure 1: Excavation Simulator System.

the joystick control law, are computed on the SPARC processor. A task-space impedance model of the excavator determines its motion as a function of a position command, a force command and an environment force. The position and force commands are generated by the action of the operator on the joystick, while the environment force is computed by the environment (ground interaction) model. Two haptic devices have been employed as an operator interface, a 6-DOF magnetically levitated (MagLev) joystick [14] and a twin pantograph device [16]. The MagLev joystick is most suited for velocity control, while the twin pantograph device, with its larger workspace, has proved useful under position command control. Force feedback determined from the interaction model, is exerted by the haptic device either as a stiffness or as a force in each of these command modes, respectively. A signal flow diagram, detailing the interaction between the haptic device, excavating machine and environment model, is shown in Figure 2. The position command control scheme is outlined in this diagram. It is clear that both commanded position and force, x_c and f_{x0}, are fed forward to the excavator, while resultant position and force, x and f_f, are fed back to the operator, via a haptic device. Each sub-system shown in Figure 2 will be described in subsequent sections. The virtual environment state is communicated to a graphics rendering sub-system, running on the SGI, through a serial port. Viewing parameters, including operator viewpoint, are adjusted through a graphical user interface.

3 Mini-Excavator Model

A Takeuchi TB035 mini-excavator, used as a research platform at UBC, has served as the model for this virtual environment. The specifications, as well as the instrumentation of this machine, are outlined in [17]. Bucket endpoint coordinates are best described, within the workspace, by means of cylindrical coordinates $\{\theta_1, r, z\}$ and bucket angle α, as shown in Figure 3. General kinematic and dynamic characteristics

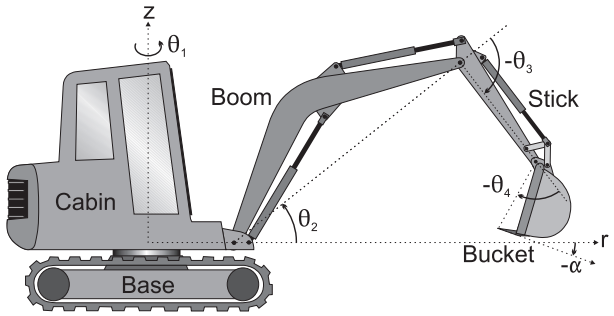

Figure 3: The Mini-Excavator, its Components and Coordinate Frames. For Bucket Details, see Figure 4.

of such machines have been presented previously in [5, 19, 6], while a specific description of the relationship between hydraulic actuator displacements, joint angles and four DOF cylindrical workspace coordinates, is described in [17]. Using position-based impedance control, the bucket endpoint dynamics in the vertical plane of the arm can be shaped into a relationship that is reasonably well approximated by (1), as described in [11].

$$M_d s^2 X = F_0 - F_e + (B_d s + K_d)(X_0 - X) \qquad (1)$$

M_d, B_d and K_d are the desired mass, damping and stiffness terms, $X = [r\, z\, \alpha]^T$ and X_0 are the actual and desired bucket position and orientation, while F_0 and F_e are the commanded and actual forces exerted by the bucket on the environment. It has been shown in [11, 12] that such impedance is indeed achievable with M_d equal to the excavator mass, and measured stiffness and damping parameters in the ranges shown in Table 1. These impedance parameters were utilised within the virtual environment as part of a discrete dynamic model based upon (1). Here, X_0, F_0 and F_e act as inputs to the model, which produces X, the actual task-space position of the excavator bucket endpoint.

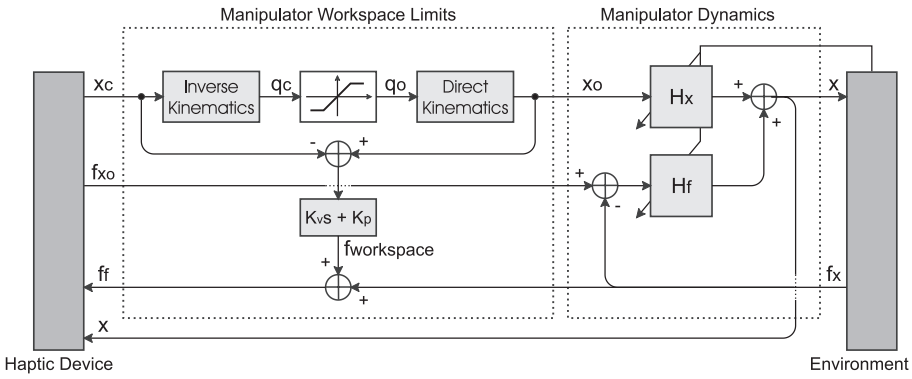

Figure 2: System Signal Flow and Control Between Master and Slave Sub-Systems.

Table 1: Experimentally determined excavator and environment impedance parameters.

Parameter	B	K
Excavator	$5000 Nm^{-1}s$	$10^4 - 10^5 Nm^{-1}$
Environment	$500 Nm^{-1}s$	$> 10^5 Nm^{-1}$

The environment damping and stiffness parameters, also shown in Table 1, were measured during actual interaction normal to a typical ground surface, and were used to guide the scaling of ground interaction model components. The environment force F_e, is dependent on the environment state, bucket position and bucket velocity.

Manipulator workspace limits are effected in joint space, as shown in Figure 2, resulting in a workspace boundary force, $f_{workspace}$. The resultant force fed back to the haptic device, is the sum of this workspace force and the computed environment interaction force. The excavator impedance can be adjusted as a function of the environment model, as discussed in [10].

4 Bucket-Ground Dynamic Interaction Model

A flat cutting surface of length s_{bucket}, which penetrates the ground surface by $s_p(r, z, \alpha)$ metres is assumed. This penetration measurement depends upon bucket endpoint depth, orientation and the existing ground surface profile, $F_u(r)$.

A ground interaction-force model has been developed, which is based upon damping, stiffness, Coulomb friction and load forces. The majority of these components have been employed and verified in other models [1, 4, 7], but are generalised here by considering arbitrary bucket angles and trajectories. Three of the four force components are computed relative to the bucket coordinate frame, which consists of normal, tangential, and orientation components, as shown in Figure 4.

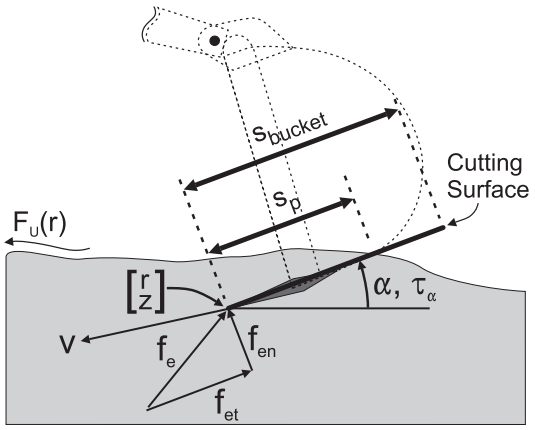

Figure 4: The Cutting Edge Frame and Dimensions.

4.1 Viscous Friction

Viscous friction between cutting and soil surfaces, due in part to adhesive properties between bucket and ground materials, results in a force which opposes motion (2,3).

$$\begin{bmatrix} f_{br} \\ f_{bz} \end{bmatrix} = -R(\alpha)\, B(r, z, s_p)\, R(\alpha)^T \begin{bmatrix} \dot{r} \\ \dot{z} \end{bmatrix} \quad (2)$$

$$\tau_b = -s_p(r, z, \alpha)\, b_{\alpha 0}\, \dot{\alpha} \ , \quad (3)$$

$$B(r, z, s_p) = \begin{bmatrix} s_p(r, z, \alpha) b_{t0} & 0 \\ 0 & s_p(r, z, \alpha) b_{n0} \end{bmatrix} \quad (4)$$

It can been seen that the damping constants are functions of contact surface area and of material properties (represented by b_{t0} and b_{n0}). The contact area is assumed to be proportional to the penetration depth, s_p.

Damping forces are expected to be greatest in the tangential bucket direction, since both the cutting surface and bucket sides contribute to viscous friction. Resistance to motion in the normal direction results from side and edge contacts. In addition, both normal forces and orientation torques may include significant damping due to environment compression.

4.2 Stiffness and Shearing Forces

A stiffness force term, (5,6), is computed relative to a stiffness centre, $\{r_c, z_c, \alpha_c\}$, where k and k_α are translational and angular stiffness factors.

$$\begin{bmatrix} f_{kt} \\ f_{kn} \end{bmatrix} = R^T(\alpha) k \begin{bmatrix} r_c - r \\ z_c - z \end{bmatrix} \tag{5}$$

$$\tau_k \quad = -k_\alpha(\alpha - \alpha_c) \tag{6}$$

Previous analysis of soil-tool behavior has suggested that soil shear failure, attributable to the breaking of cohesive bonds within the ground, should be included within the cutting force model [4, 7], as shown in Figure 5. Here it is assumed that displacement of the

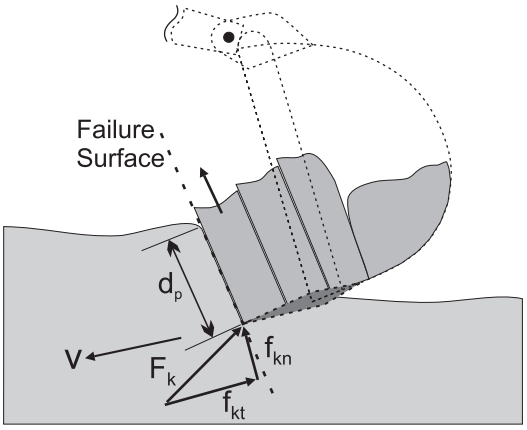

Figure 5: Stiffness Force Components Which Lead to Soil Shearing.

soil results in simultaneous failure along a planar surface within the ground. This surface extends from the bucket tip to the ground surface at an angle which is related to cutting edge form, orientation and soil properties. In general, this failure surface is complex [7], therefore we consider that the accumulation of force normal to the cutting surface, due to soil stiffness, will eventually result in such failure. This has been implemented by maintaining an estimate of perpendicular shearing force, Swd_p, where w is the bucket width, S is a soil characteristic and d_p is the perpendicular distance from bucket tip to soil surface. Shearing occurs as soon as the opposing normal bucket force equals, or exceeds the current shearing force threshold, that is:

$$\text{If } f_{kn} \geq Swd_p, \text{ then } \quad \begin{bmatrix} r_c \\ z_c \end{bmatrix} = \begin{bmatrix} r \\ z \end{bmatrix} \tag{7}$$

At this time, soil stiffness is relieved and the centre of stiffness is reset to the current bucket endpoint position. The ground surface profile $F_u(r)$, shown in Figure 6, is also updated to reflect the change in soil surface dimensions.

In [7] the distance between subsequent failures has been shown to be dependent only upon cutting edge depth and is implemented by modulating a soil cohesion factor via a depth dependent *sawtooth* function. In contrast, in equation (7), both bucket position and orientation (including depth) account for periodic soil failures in a clear, physically intuitive manner.

4.3 Bucket Load Accumulation Forces

Accumulated material within the bucket results in two force components, namely load weight and accumulation force. The latter results primarily from churning effects of soil caught within the bucket [1], as shown in (8,9).

$$\begin{bmatrix} f_{lr} \\ f_{lz} \end{bmatrix} = \begin{bmatrix} \epsilon \cdot V_{load} \\ -\rho \cdot g \cdot V_{load} \end{bmatrix} \tag{8}$$

$$\tau_{l\alpha} = \frac{1}{2} s_{bucket}(f_{lz} \cos\alpha - f_{lr} \sin\alpha) \tag{9}$$

Here, ρ represents soil density, $-g$ is acceleration due to gravity and V_{load} is the volume of soil accumulated within the bucket, computed according to (10):

$$V_{load}(t) = \int_{r(t)}^{r_{max}} w(F_u(r) - z(t))dr \ , \tag{10}$$

where $(F_u(r) - z(t))$ is the bucket endpoint depth below the ground surface at time t. This surface profile is updated as the bucket moves through the earth, accumulating material, as shown in Figure 6. The soil accumulation force is modelled as being proportional to bucket soil volume with ϵ being a bucket geometry characteristic. Orientation torque, $\tau_{l\alpha}$, is computed from the resulting normal load force component which is assumed to act at the centre of the cutting edge, s_{bucket}.

4.4 Coulomb Friction

Soil-bucket contact force normal to the cutting surface results in a resistive force which opposes tangential bucket motion. This force has been modelled as Coulomb friction (11):

$$f_{ct} = -\mu \frac{v_t}{|v_t|} |f_{bn} + f_{kn} + f_{ln}| \ , \tag{11}$$

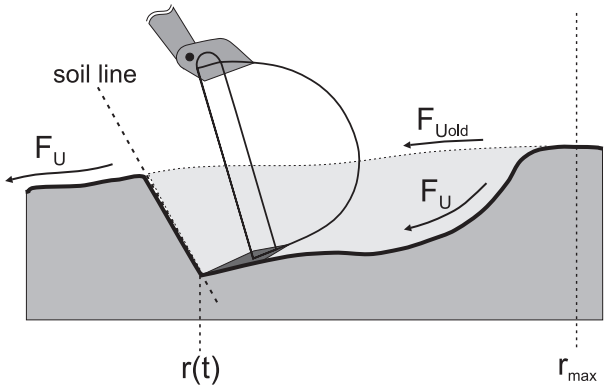

Figure 6: Ground Surface Dimensions are Updated and Stored in $F_u(r)$.

where μ is the coefficient of friction between soil and bucket and v_t is the tangential bucket velocity.

4.5 Combining Interaction Forces

Each of the four bucket-ground interaction forces presented in this section includes one or more factors which are determined by both bucket and soil characteristics. It is likely that the soil moisture content and consistency play an important role in determining relative magnitudes of component interaction forces. For instance shearing, traditionally a feature of metallic and crystalline solids, is most applicable to dryer, more brittle ground material. Conversely, a moist, fine soil would present more viscous properties, with little stiffness, but high damping. The model proposed herein is most suited to hard, dry earth.

The relative magnitude of each force component was adjusted experimentally in order to obtain an intuitive environment feel during excavation.

Figure 7 shows estimated environmental interaction forces for two different angles of attack, α, namely 10° (shown in A) and 40° (shown in B); and similar bucket endpoint trajectories. The larger bucket angle results in a greater environment force in the radial direction and a slightly smaller vertical force upon descent. Radial force is particularly sensitive to excavation depth, due to increased cutting edge penetration. The weight of accumulated soil is evident in (A), where the small bucket angle results in trapped soil within the bucket.

The interaction force model presented in this section is used as feedback to the excavator dynamics and depends only upon environment and excavator states, thus avoiding any algebraic loops within the force model.

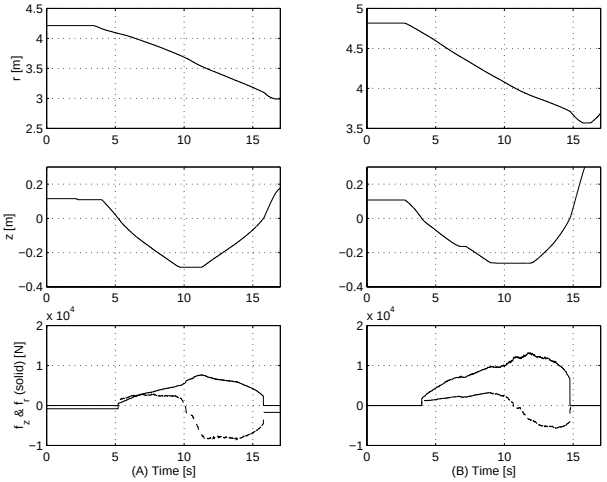

Figure 7: Ground Interaction Force Estimates for Two Angles of Attack. In (A), $\alpha = 10°$ and in (B), $\alpha = 40°$.

4.6 Force Model Extensions

The effect of angular motion upon forces and torques is more accurately modelled by integrating force and torque contributions along the submerged cutting surface, s_p. At present we have considered only a flat cutting surface, however any arbitrary bucket geometry could be accomodated through force integration.

In addition, interaction force and torque components should be integrated over the entire bucket width, since the ground surface profile, $F_u(r)$, may vary significantly along the cutting edge.

Soil-soil friction along the failure plane, and soil wedge weight and inertia should also be considered.

5 Graphical Simulator

Visual feedback is delivered with an SGI workstation equipped with the VGX graphics engine. Both the excavator model and dynamic environment are displayed within a realistic, yet responsive visual environment. IRIS Performer^{TM}, a graphics library built upon OpenGL, was used to implement a scene rendering pipeline, complete with a graphical user interface. The primary design issues in the construction of this graphical environment were, (i) the modelling and animation of an articulated excavator manipulator; and (ii) the implementation of a dynamic, deformable digging environment. Rough scale models of each of the five excavator components were drafted individually and assembled as a hierarchy of dynamic coordinate systems, within the graphics scene tree. The excavator configuration is provided to the graphical environment in terms of workspace coordinates, by the real-time

system, via a serial communications interface. Joint angles, computed using inverse excavator kinematics, are used to orient each manipulator link with respect to the previous link frame, taking advantage of coordinate system hierarchy.

The world environment consists of a ground plane which is capable of deformation during digging. As the excavator bucket removes soil from the ground, a trench is generated within this plane, complete with textured soil, clearly reflecting environment state to the operator. A polygonal mesh-based ground plane proved to be prohibitively expensive, in terms of rendering time. Because of this, it is necessary to expand the trench by adding polygonal modules, as required. A three polygon module, shown in Figure 8, is added as the bucket tip makes progress through the ground. Although this technique does produce a real-

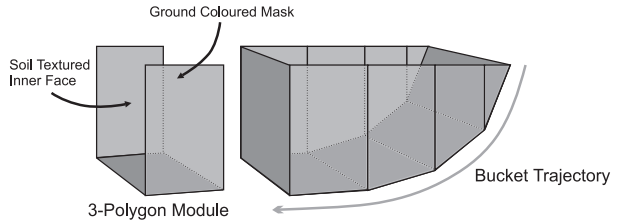

Figure 8: The textured polygonal modules which are added while constructing an excavation trench.

istic looking trench, it does still require the generation of a hole within the ground plane. This has been implemented by rendering the trench graphics in front of the ground plain, leaving the trench visible despite being submerged below ground level. This is achieved by clearing the depth buffer (z-buffer) after ground plane generation, but prior to trench rendering, effectively forcing the ground plane to the back of the scene. The outer faces of the trench are hidden by using ground plane colouring, while the inner faces are appropriately textured.

Additional features, such as a shadow and soil which falls to the ground as the bucket is relieved of its load, have been included in order to provide the operator with valuable depth cues, and to enhance visual feedback realism. Figure 9 shows both the graphical excavator and environment during digging.

6 Conclusions and Future Work

This paper has outlined the implementation of a virtual excavation environment which includes both realistic visual feedback, as well as force feedback derived from a new ground interaction model, for the purposes of controller design and performance evaluation. In addition to this, an impedance model has been included in order to describe excavator dynamics. This has allowed for the testing and evaluation of various impedance-based teleoperation strategies currently under development and evaluation at the University of British Columbia [10]. Other applications, such as operator training and evaluation, and excavation trajectory programming, would also benefit from such a virtual environment equipped with interaction force feedback.

Further refinement and tuning of the ground interaction model, with reference to validation data, is necessary in order to obtain a qualitatively accurate "feel", perhaps in the presence of variable ground characteristics and submerged obstacles. It may also become necessary to model non-linear dynamic effects currently observed in the real excavator, including deadbands, hysteresis and other effects which are not eliminated by its position-based impedance controller.

7 Acknowledgments

This work was supported by the Canadian IRIS/PRECARN Network of Centers of Excellence, project IS-4.

References

[1] T.V. Alekseeva, K.A. Artem'ev, A.A. Bromberg, R.I. Voitsekhovskii, and N.A. Ul'yanov. *Machines for Earthmoving Work - Theory and Calculations.* Mashinostroenie Publishers, Moscow, 1972.

[2] A.K. Bejczy and W.S. Kim. Predictive Displays and Shared Compliance Control for Time Delayed Telemanipulation. *Int. Workshop on Intelligent Robots and Systems*, July 1990.

[3] Antal K. Bejczy, Paolo Fiorini, Won Soo Kim, and Paul Schenker. Toward Integrated Operator Interface for Advanced Teleoperation under Time-Delay. *Proc. Int. Conf. on Intelligent Robots and Systems*, pages 563–570, 1994.

[4] Leonard E. Bernold. Experimental Studies of Mechanics of Lunar Excavation. *J. of Aerospace Eng.*, 4(1):9–22, January 1991.

[5] A.J. Koivo. Kinematics of Excavators(Backhoes) for Transferring Surface Material. *J. of Aerospace Eng.*, 7(1):17–32, January 1994.

[6] A.J. Koivo, M. Thoma, E. Kocaoglan, and J. Andrade-Cetto. Modeling and Control of Excavator Dynamics During Digging Operation. *J. of Aerospace Eng.*, pages 10–18, January 1996.

[7] F. Malaguti. Soil Machine Interaction in Digging and Earthmoving Automation. *Proceedings of the* 11^{th} *International Symposium on Automation and Robotics in Construction*, pages 187–192, 1994.

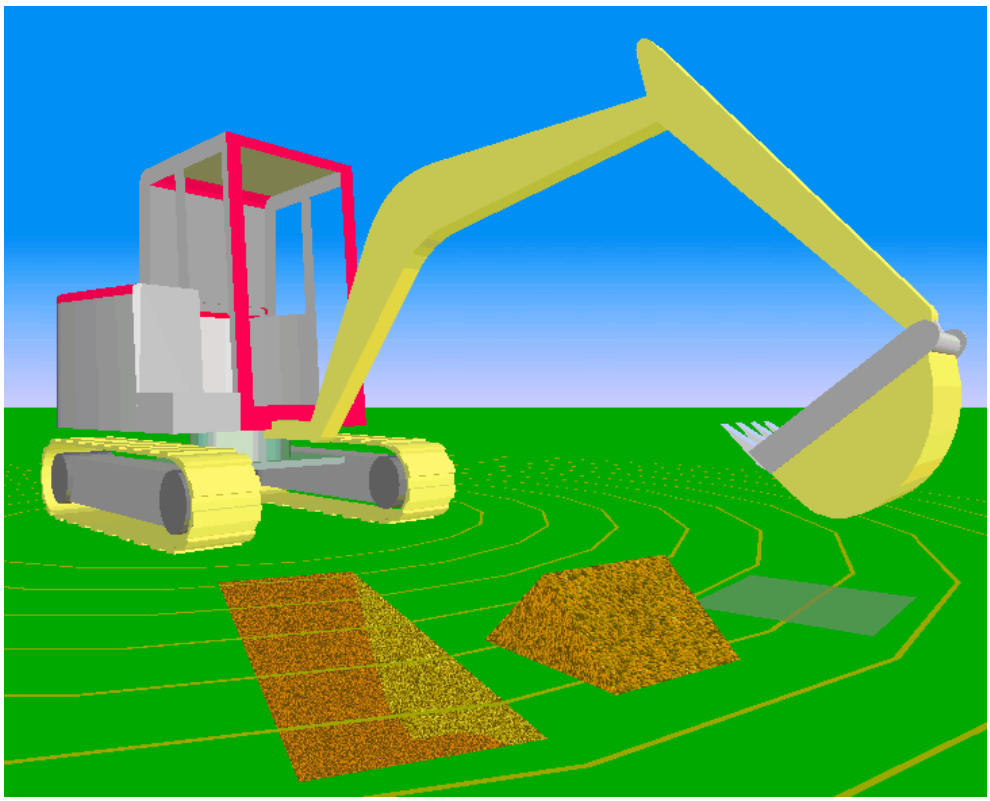

Figure 9: A Screen Snapshot of the Visual Environment.

[8] N.R. Parker, S.E. Salcudean, and P.D. Lawrence. Application of Force Feedback to Heavy Duty Hydraulic Machines. In *Proc. IEEE Int. Conf. on Rob. and Auto.*, pages 375–381, Atlanta, USA, May 1993.

[9] R. Langreth. Smarter Shovel. *Popular Science*, 240(6):82–84, 108–109, 1992.

[10] S.E. Salcudean, K. Hashtrudi-Zaad, S. Tafazoli, S.P. DiMaio, and C. Reboulet. Bilateral Matched Impedance Teleoperation with Application to Excavator Control. *IEEE International Conference on Robotics and and Automation*, 1998.

[11] S.E. Salcudean, S. Tafazoli, K. Hashtrudi-Zaad, P.D. Lawrence, and C. Reboulet. Evaluation of Impedance and Teleoperation Control of a Hydraulic Mini-Excavator. *Proc. 5^{th} Int. Symp. on Experimental Robotics*, June 1997.

[12] S.E. Salcudean, S. Tafazoli, P.D. Lawrence, and I. Chau. Impedance Control of a Teleoperated Mini Excavator. *Int. Conf. for Advanced Robotics '97*, July 1997.

[13] S.E. Salcudean, P. Drexel, D. Ben-Dov, and P.D. Lawrence. A Six-Degree-of-Freedom, One Person, Hydraulic Motion Simulator. In *Proc. IEEE Intl. Conf. Rob. Automat.*, pages 2437–2443, San Diego, California, May 9-12 1994.

[14] S.E. Salcudean, N.M. Wong, and R.L. Hollis. Design and Control of a Force-Reflecting Teleoperation System with Magnetically Levitated Master and Wrist. *IEEE Transactions on Robotics and Automation*, 11(6):844–858, December 1995.

[15] Sanjiv Singh. Learning to Predict Resistive Forces During Robotic Excavation. *International Conference on Robotics and Automation*, pages 2102–2107, 1995.

[16] L. Stocco, S. E. Salcudean, and F. Sassani. Mechanism Design for Global Isotropy with Applications to Haptic Interfaces. In *Proc. ASME Winter Annual Meeting*, pages 115–122, Dallas, Texas, November 1997.

[17] Shahram Tafazoli. *Identification of Frictional Effects and Structural Dynamics for Improved Control of Hydraulic Manipulators*. PhD thesis, University of British Columbia, January 1997.

[18] U. Wallersteiner, P. Stager, and P.D. Lawrence. A Human Factors Evaluation of Teleoperated Hand Controllers. In *International Symposium on Teleoperation and Control*, Bristol, England, July 1988.

[19] P.K. Vähä and M.J. Skibniewski. Dynamic Model of Excavator. *J. of Aerospace Eng.*, 6(2):148–158, April 1993.